Anisotropic Alignment of Lamellar Potassium Hexaniobate Microcrystals and Nanoscrolls in a Static Magnetic Field

Miharu Eguchi,[†] Mark S. Angelone,[‡] Hemant P. Yennawar,[†,§] and Thomas E. Mallouk*[,†]

Department of Chemistry, Materials Research Institute, Department of Biochemistry and Molecular Biology, The Pennsylvania State University, University Park, Pennsylvania 16802

Received: March 28, 2008

Microcrystals of potassium hydrogen hexaniobate ($K_{1.8}H_{2.2}Nb_6O_{17}\cdot nH_2O$) and nanoscrolls derived from them were suspended in an aqueous solution of tetramethyl orthosilicate and then subjected to a static homogeneous 11.74 T magnetic field as the silicate solution formed a gel. After supercritical drying of the gels, samples were studied by conventional 1D powder X-ray diffraction (XRD) in $\theta-\theta$ geometry and by 2D XRD in a Debye−Scherrer geometry. Analysis of the XRD data from the field-aligned microcrystals shows that they are oriented with their crystallographic *a*-axis along the field direction, with an order parameter of approximately 0.9. The stacking axis of the layered solid (the *b* axis) is thus oriented perpendicular to the applied field. With the nanoscrolls, the 2D XRD pattern showed some evidence of some preferred orientation along the long axis of the scrolls, which could not be quantified because of the crystallographic heterogeneity of the nanoscrolls. Optical birefringence of the field-aligned nanoscroll samples was also observed. The edge-on orientation of lamellar crystals and vertical orientation of tubes and scrolls is difficult to achieve by other means and is of potential interest for membranes that exploit the in-plane transport properties of lamellar solids.

Introduction

Lamellar solids such as graphite, clays, layered transition metal oxides, and layered chalcogenides have highly anisotropic physical properties that are a consequence of strong chemical bonding in two rather than three crystallographic directions. Some of the interesting anisotropic properties of layered compounds include their mechanical strength, optical absorption and reflectivity, and the transport behavior of electrons, holes, and intercalated ions. As a consequence of this underlying anisotropy, the properties of composite materials that contain particles or exfoliated sheets of layered solids are strongly dependent on the orientation and organization of the lamellae.

One such property that is of substantial practical interest is ionic conductivity. The in-plane proton conductivities of some lamellar metal phosphates and layer perovskites in their acid-exchanged forms are within 1 order of magnitude of those of the proton-conducting polymers used in polymer electrolyte membrane (PEM) fuel cells.[1–7] In the layered solids, the conductivity perpendicular to the plane of the sheets is usually several orders of magnitude lower than in plane.[8] Because inorganic solids are stable to higher temperature than organic polymers, they are interesting candidate electrolytes for fuel cells that could function above the maximum temperature (150−200 °C) of polymer-based cells.[9,10] Unfortunately, the techniques that are used to make membranes from layered solids, such as casting suspensions of particles or exfoliated sheets,[11] cause the conducting direction to be preferentially oriented in the membrane plane.[8,12] To exploit the properties of these materials as ionically conducting membranes, techniques must be devised for orienting the sheets perpendicular to the membrane plane. So far there are no general methods for achieving this edge-on orientation in membranes and thin films.

It is now well-known that strong homogeneous magnetic fields can be used to achieve controlled orientation of particles in fluid suspensions and that these oriented particles can be consolidated to make composites and thin films.[13–21] With diamagnetic materials, this effect is dependent on the anisotropy of the magnetic susceptibility, $\Delta\chi$, as described by eq 1, in which $\Delta\chi = \chi_{||} - \chi_{\perp}$ and μ_0 is the vacuum permeability. In the parallel direction, the crystal axis of highest χ is aligned with the applied magnetic field

$$\Delta E = \frac{\Delta\chi V B^2}{2\mu_0} \tag{1}$$

To orient the particles, the energy difference (ΔE) between the parallel and perpendicular orientations must be much larger than the thermal energy kT. Because ΔE is proportional to the particle volume (V) and the square of the field strength (B), the field strength needed to overcome thermal randomization of the orientation in fluids is strongly size-dependent. Magnetic fields on the order of several Tesla are ordinarily needed to orient nanoparticles, but lower fields (~1 T) that are more readily accessible in the laboratory are adequate for micrometer-size particles. Anisotropic materials that contain one or two long axes (such as crystal platelets, nanotubes, and nanorods) represent an interesting intermediate case because they have both nanoscale and microscale dimensions. Previous studies on the interaction of mica crystallites with magnetic fields have shown that they can be aligned with the layer axis perpendicular to the applied field.[22] Uyeda and co-workers have studied tetrahedrally and octahedrally coordinated oxides,[23–25] and their analysis of the diamagnetic anisotropy of individual bonding orbitals suggests that in many cases the preferential alignment direction for lamellar solids should be edge-on, i.e., in the desired arrangment for proton conducting membranes.

* To whom correspondence should be addressed. E-mail: tom@chem.psu.edu.
[†] Department of Chemistry, The Pennsylvania State University.
[‡] Materials Research Institute, The Pennsylvania State University.
[§] Department of Biochemistry and Molecular Biology, The Pennsylvania State University.

10.1021/jp802702m CCC: $40.75
Published on Web 07/08/2008

In this paper, we report the magnetic alignment of the lamellar compound $K_{4-x}H_xNb_6O_{17}\cdot nH_2O$ ($x \approx 2.2$). Because this compound can be studied both as micrometer-sized platelike crystals,[26,27] and as scrolled, exfoliated nanosheets,[28–30] it presents an interesting case for studying the magnetic alignment of a layered diamagnetic proton conductor in microscale and nanoscale forms. With the lamellar microcrystals, the crystallographic *a* axis, which lies in the plane of the sheets, orients along the magnetic field direction. A high degree of preferred orientation, quantified by two-dimensional X-ray diffraction (2D XRD), can be achieved in sol−gel composites that are solidified in the bore of an NMR magnet (a 11.74 T homogeneous magnetic field). With the nanoscale scrolls, which are approximately 30 nm in diameter and 0.5−1 μm long, there is also evidence of preferred orientation, although it appears to be much weaker than in the case of the microcrystals.

Experimental Methods

Synthesis and analysis of $K_4Nb_6O_{17}$ and $K_{4-x}H_xNb_6O\cdot nH_2O_{17}$. Potassium hexaniobate ($K_4Nb_6O_{17}$) was synthesized as follows: 1.95 g of K_2CO_3 and 5.12 g of Nb_2O_5 were mixed and ground finely with an agate mortar and pestle. A 10% stoichiometric excess of K_2CO_3 was added to compensate for loss of volatile K_2O at the reaction temperature. The powder mixture was calcined in a covered alumina crucible, which was ramped from 25 to 1200 at 20 °C/min and held at the maximum temperature for 15 min. The white crystalline product so obtained was ground finely with an agate mortar and pestle and analyzed by powder XRD. By comparison with previously published patterns, the product was identified as the trihydrate, $K_4Nb_6O_{17}\cdot 3H_2O$. Diffraction patterns of the starting material (Nb_2O_5) and likely impurity phases ($KNbO_3$ and $K_6Nb_{11}O_{23}$) were not observed. The $K_4Nb_6O_{17}\cdot 3H_2O$ powder (approximately 6 g) was proton-exchanged by dispersion in 100 mL of 0.25 M aqueous H_2SO_4 and stirring for 24 h. The solid product ($K_{4-x}H_xNb_6O_{17}\cdot nH_2O$) was repeatedly centrifuged and washed with water until the supernatant became pH neutral, and the solid product was then dried at 60 °C. The product was analyzed for K and Nb by inductively coupled plasma atomic emission spectroscopy (ICP-AES) on a Perkin-Elmer Ultima 5300 instrument. For K analysis, samples were dissolved by lithium metaborate fusion, and Rock standards were used to calibrate the results. For Nb, samples were dissolved by sodium peroxide fusion, and synthetic standards were used for calibration.

Synthesis of Hexaniobate Nanoscrolls. Scrolled exfoliated sheets of the lamellar hexaniobate were prepared as described elsewhere.[28,30] Powdered $K_{4-x}H_xNb_6O_{17}\cdot nH_2O$, 3 g, was dispersed in 100 mL of 2.6 M aqueous tetra(*n*-butylammonium) hydroxide, TBA^+OH^-, and stirred for 24 h. The portion of the sample that was not completely suspended was discarded, and the solid from the well-suspended fraction was collected by centrifugation and redispersed in water. The sample was centrifuged and resuspended in water several times until the pH of the supernatant was neutral. The solid recovered by centrifugation was dried in air at 60 °C.

Magnetic Alignment, Solidification, and Drying of Hexaniobate Dispersions. To fix the magnetically induced alignment of the lamellar crystals and nanoscrolls for subsequent structural analysis, an in situ sol−gel reaction was used. Tetramethoxysilane ($Si(OMe)_4$, TMOS) (Gelest, Inc.), 200 μL, was mixed with 20 μL of 0.01 M HCl and 30 μL of water (TMOS:water = 1:2 (stoichiometric ratio)) and stirred for 15 min until hydrolysis had partially occurred and the two liquids became miscible. 50 mg of the solid microcrystals or nanoscrolls, which was dispersed and stirred 24 h in 1 mL water in advance of the TMOS reaction, was added to partially hydrolyzed TMOS solution. The mixture was placed in a 10 mm diameter borosilicate NMR tube. For powder XRD, 2D XRD, and optical birefringence experiments, gelled samples with smooth flat surfaces were needed. This was achieved by fabricating a rectangular glass container (7 mm × 18 mm × 1 mm) from glass microscope slides, coverslip spacers, and double-sided adhesive tape. This container was loaded vertically into the NMR tube before adding the $K_{4-x}H_xNb_6O_{17}\cdot nH_2O$/TMOS mixture.

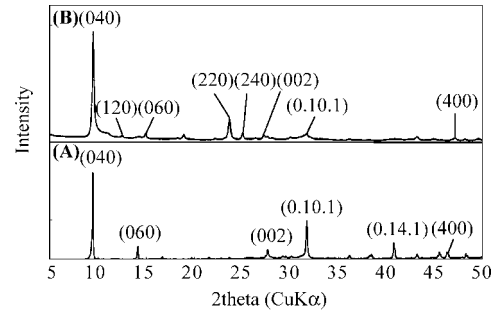

Figure 1. XRD patterns of (A) $K_4Nb_6O_{17}\cdot 3H_2O$ and (B) $K_{1.8}H_{2.2}Nb_6O_{17}\cdot nH_2O$.

The NMR tube containing the sample and the inner container was introduced into the static magnetic field (11.74 T) of a Bruker AMX-2−500 MHz NMR with an Oxford magnet and kept there at 19 °C for 24 h to complete the sol−gel reaction. An identically prepared sample was gelled outside of the magnetic field, and a control sample containing only the TEOS mixture and no $K_{4-x}H_xNb_6O_{17}\cdot nH_2O$ was gelled under the same conditions in the field. The sample in the inner container was removed from the NMR tube and subjected to supercritical drying using a BAL-TEC CPD030 apparatus. The water in the gel was replaced gradually by soaking the sample sequentially in ethanol/water mixtures containing 15, 20, 35, 50, 75, 85, 95, 100% ethanol. The ethanol was replaced with liquid CO_2 at 5.4×10^6 Pa in the specimen pressure chamber. The pressurized sample was heated above the CO_2 critical temperature (31 °C, 7.38×10^6 Pa), and the pressure was then reduced to obtain the dried sample.

Powder X-Ray Diffraction. Two instruments were used to obtain 2D XRD patterns of gelled samples. A Rigaku D/max Rapid II instrument (Mo Kα, 50 kV, 40 mA) was used to obtain qualitative data and index the diffraction patterns, and a Bruker Smart Apex detector (Cu Kα, 50 kV, 40 mA) was used to obtain quantitative data for analysis of azimuthal scans. A Philips X'pert-MPD (Cu Kα, 40 kV, 40 mA) instrument was used to obtain ordinary 1D XRD patterns in θ-θ geometry.

Results and Discussion

Proton Exchange of $K_4Nb_6O_{17}\cdot 3H_2O$ Microcrystals. ICP-AES analysis of the dried acid-exchanged microcrystalline sample gave 7 ± 1 and 54 ± 3% K and Nb, respectively. This analytical K/Nb ratio corresponds to a stoichiometry of $K_{1.8}H_{2.2}Nb_6O_{17}\cdot nH_2O$ (theor: 8% K, 62% Nb for the anhydrous compound). This is consistent with earlier reports that acid exchange under mild conditions leads primarily to proton exchange in one of the two crystallographically distinct bilayer galleries of $K_4Nb_6O_{17}$.[31]

The XRD patterns of $K_4Nb_6O_{17}\cdot 3H_2O$ and the acid-exchanged product $K_{1.8}H_{2.2}Nb_6O_{17}\cdot nH_2O$ are compared in Figure 1. Sharp 0*k*0 layer lines are observed for $K_4Nb_6O_{17}$. The

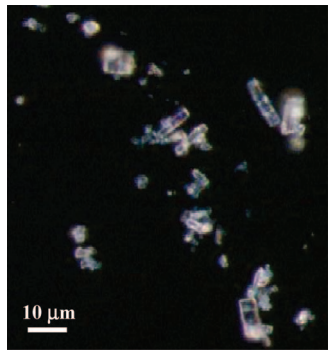

Figure 2. Optical microscope image of proton-exchanged $K_{1.8}H_{2.2}Nb_6O_{17}\cdot nH_2O$ microcrystals.

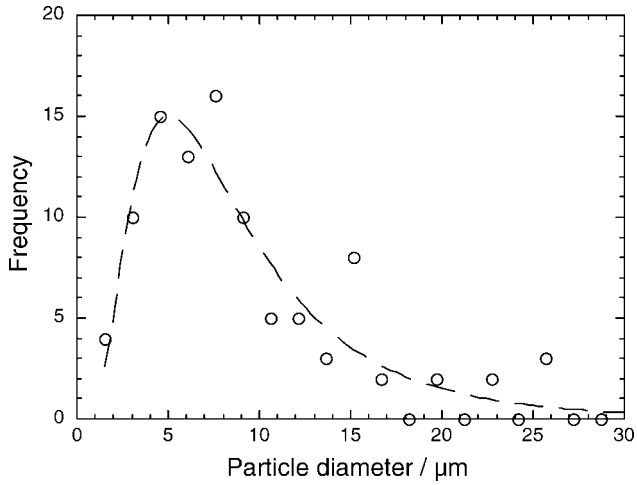

Figure 3. Histogram of the lateral dimensions of lamellar $K_{1.8}H_{2.2}Nb_6O_{17}\cdot nH_2O$ particles. Dashed line is a fit to a log-normal particle size distribution.

XRD pattern of the product (Figure 1B) shows a similarly sharp 040 diffraction line, but higher-order 0*k*0 lines are weaker, consistent with some loss of order along the stacking axis. The proton-exchanged material also has a prominent 220 reflection that is weak in the parent material. Optical microscope images confirm that particles of the acid-exchanged product retain the tabular morphology of the microcrystalline precursor material (Figure 2).

The distribution of longest dimensions of particles, obtained from optical micrographs, is shown in Figure 3. The particle lengths range from 1−2 μm to ∼30 μm, and the maximum in the distribution occurs around 5 μm. Because the particles are 1−7 μm in thickness, their volume is in the range of 10 μm^3 or larger. Kimura has calculated that particles in this size range with typical values of $\Delta\chi$ can be oriented in magnetic fields of a few Tesla.[32]

Synthesis and Characterization of Nanoscrolls. Atomic force microscopy and transmission electron microscopy (TEM) images of the hexaniobate nanoscrolls were consistent with those published previously.[28–30] Their average diameter was 20−30 nm, and their length was a several hundred nanometers. The volume of these scrolls is on the order of 4×10^{-4} μm^3, suggesting that very strong magnetic fields will be needed to induce orientational order.[32] XRD patterns (Figure 4) show broad 020 and 040 reflections, consistent with the small number of unit cell repeats along the stacking axis in the individual scrolls. Apart from these layer lines, the most prominent reflections are (002) and (400), which are expected to be strong for scrolls that have the crystallographic *c* and *a* axis as their

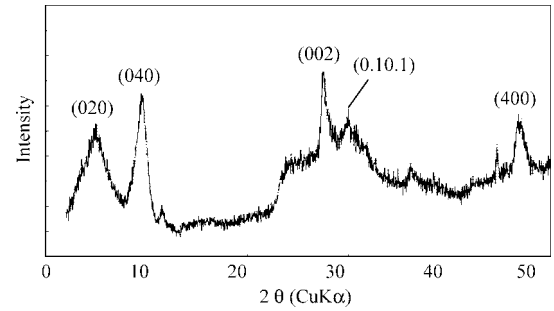

Figure 4. Powder XRD pattern of hexaniobate nanoscrolls.

long directions, respectively. This is consistent with our earlier conclusion, from analysis of TEM images, that the hexaniobate sheets tend to scroll along low-index crystal directions.[28]

XRD Analysis of Magnetically Aligned Samples. Both 2D XRD analysis in transmission mode and conventional 1D XRD data were used to determine the orientation of magnetically aligned $K_{1.8}H_{2.2}Nb_6O_{17}\cdot nH_2O$ microcrystals and nanoscrolls. The instrumental configuration shown in Figure 5A was used to record full Debye−Scherrer diffraction rings on a cylindrical image plate detector. The distribution of intensity in the diffraction rings reflects the orientation distribution of crystal planes. The transmission method is well suited for the study of uniaxial texture in sheet like specimens when the orientation axis is aligned in the plane of the sheet[33,34]

The 2D XRD patterns of microcrystalline $K_{1.8}H_{2.2}Nb_6O_{17}\cdot nH_2O$ samples gelled with and without an applied 11.74 T field are shown in parts B−D of Figure 5. The zero-field sample shows homogeneous diffraction rings (Figure 5B), indicating that there is minimal preferred orientation. In contrast, the sample that was gelled in the field shows bright diffraction arcs and spots (parts C and D of Figure 5). These features, which are indicative of magnetic alignment, can be indexed according to the powder diffraction pattern in Figure 1B. In parts B and C of Figure 5, the direction of the applied magnetic field is in the *y* direction and approximately parallel to the direction of the beam stop, which appears as a dark shadow in the image, and the X-ray beam was perpendicular to the sample plane which is shown in yellow in Figure 5A. In this configuration, diffraction can be observed from planes with normals inclined by their Bragg angle (θ) to the plane of the sheet and at any angle of rotation (ϕ) about the beam axis. The arcs of high intensity on the *x* axis (d = 9.4 Å, (040); d = 3.2 Å, (002)) correspond to plane normals for those reflections that are preferentially oriented perpendicular in ϕ to the magnetic field. The arcs on the *y* axis (d = 1.9 Å, (400)) correspond to 400 normals preferentially oriented parallel in ϕ to the field. The appearance of 0*k*0 and 00*l* reflections as sharp diffraction spots along the *x* axis and *h*00 reflections as arcs along the *y* axis suggests an orientation of the crystallographic *a* axis aligned in the direction of the applied field and a symmetric random orientation about the *a* axis, that is, a uniaxial orientation.

To confirm the uniaxial distribution, the specimen was mounted with X-ray beam perpendicular to and impinging on the edge of the sample sheet (shown as the white edge of the sample in Figure 5A) and with the applied magnetic field direction parallel to the *x* axis. In this configuration, diffraction can be observed from planes with normals inclined by an angle of θ to the edge of the sheet and in any angle of rotation (ϕ) about the beam axis. The diffraction pattern in Figure 5D shows high intensity arcs on the 400 Debye ring aligned in the plane of the sheet. This further indicates a uniaxial distribution of the

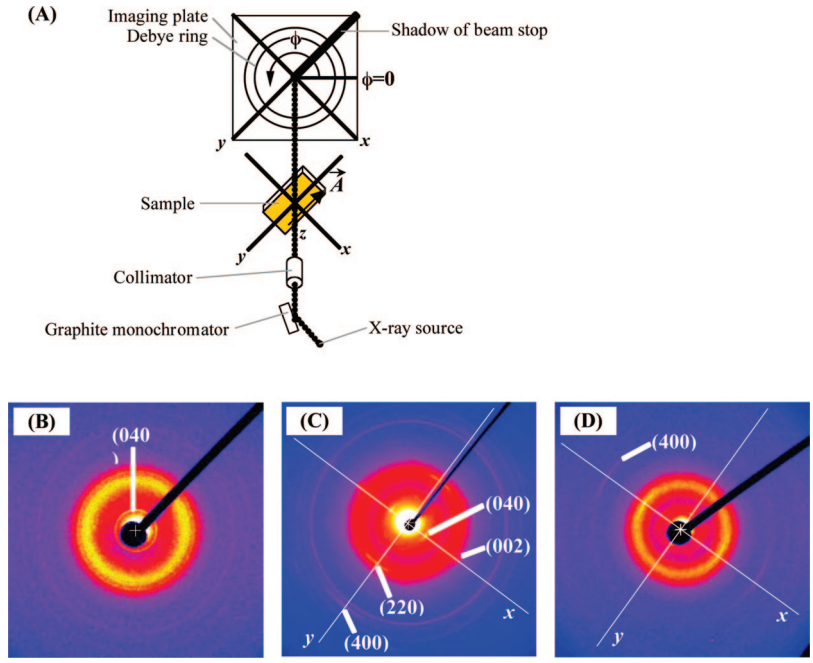

Figure 5. 2D XRD patterns of $K_{1.8}H_{2.2}Nb_6O_{17}\cdot nH_2O$/silica gel. (A) The experimental arrangement of the sample, X-ray beam and imaging plate. ϕ is the rotational angle about the beam axis. Vector A shows the direction of the applied magnetic field. Sample gelled (B) in zero magnetic field, and (C, D) in a 11.74 T field. The incident X-ray beam was perpendicular to the face of the sample in C and perpendicular to the edge of the sample in D.

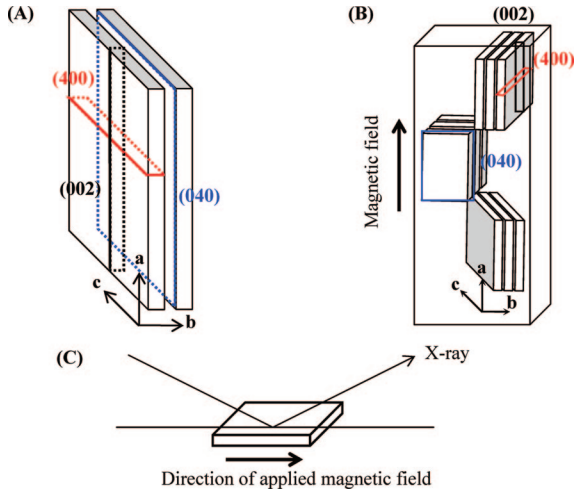

Figure 6. Geometric relation of (A) $K_{1.8}H_{2.2}Nb_6O_{17}\cdot nH_2O$ structure and lattice planes indexed in Figure 5 and (B) lattice planes and the direction of the applied magnetic field. (C) Sample orientation for 1D XRD experiments.

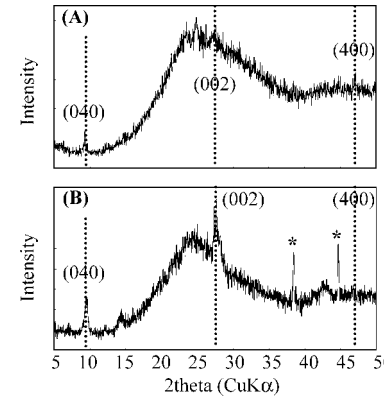

Figure 7. Powder XRD patterns of $K_{1.8}H_{2.2}Nb_6O_{17}\cdot nH_2O$/silica samples gelled (A) in a 11.74 T field and (B) in a zero field. Asterisks indicate background diffraction lines from the aluminum sample mount.

a axis in the plane of the sheet and aligned in the field direction rather than askew of the sheet, or in a multinodal or other complex biaxial alignment. The dominant orientation of $K_{1.8}H_{2.2}Nb_6O_{17}\cdot nH_2O$ crystallographic planes as described here is illustrated in parts A and B of Figure 6.

The same measurement was performed on a sample that contained the sol−gel reagents but did not include $K_{1.8}H_{2.2}Nb_6O_{17}\cdot nH_2O$, and only isotropic diffuse diffraction rings were observed. This confirms that the observed diffraction arcs and spots are a consequence of magnetically induced alignment of the $K_{1.8}H_{2.2}Nb_6O_{17}\cdot nH_2O$ microcrystals.

To confirm the field-induced orientation of the microcrystals, the same samples were studied by conventional 1D powder XRD in a $\theta-\theta$ geometry, as shown in Figure 6C. The diffraction pattern is shown in Figure 7, with an expanded view of the region of the (400) reflection in Figure 8. The sharp Bragg diffraction lines of the microcrystals are superimposed on the broad envelope of diffraction from the amorphous silica gel. It is evident from Figure 6 that the (040) and (002) reflections are stronger, relative to the background in the sample gelled in the magnetic field. On the other hand, the (400) reflection is clearly observable in the zero field sample but absent in the field-aligned sample. This is consistent with the orientation of lattice planes shown in Figure 6. In the field-aligned sample, both the crystallographic *b* and *c* axes can be oriented in the plane of the sample holder, and therefore their intensity is enhanced relative to a randomly oriented sample. However, the *a* axis is oriented in the magnetic field direction, which is perpendicular to the plane of the sample holder. Thus the *h*00 reflections are not observed in the field-aligned sample.

Estimation of the Orientation Parameter of Field-Aligned $K_{1.8}H_{2.2}Nb_6O_{17}\cdot nH_2O$ Microcrystals. Quantitative 2D XRD intensity data acquired on a Rigaku DMAX system with Mo Kα radiation (Figure 9) were used to estimate the orientation parameter of the field-aligned microcrystals. The degree of preferred orientation in uniaxial alignments is conveniently

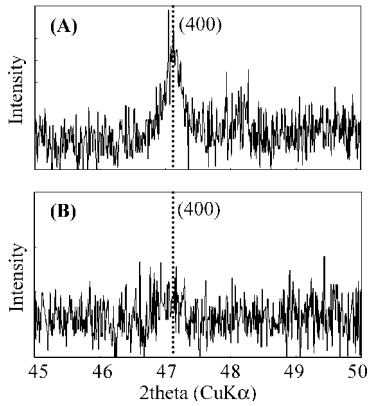

Figure 8. Powder XRD in the $2\theta = 45-50°$ region of $K_{1.8}H_{2.2}Nb_6O_{17}\cdot nH_2O$/silica samples gelled (A) in a 11.74 T field and (B) in a zero field.

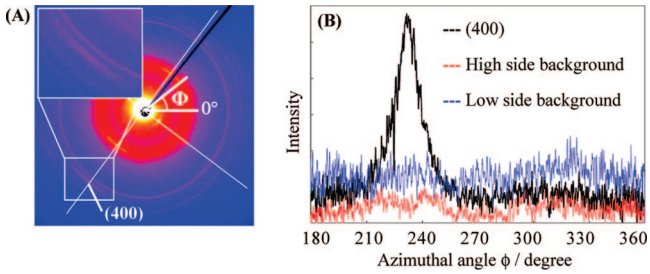

Figure 9. 2D XRD intensity distribution as a function of azimuthal angle. (A) Azimuthal distribution of the (400) diffraction line, plotted from $\phi = 180$ to 360°. (B) Intensity of the (400) reflection (black line) vs azimuthal angle. Background intensities on the high (red line) and low (blue line) angle sides of the Bragg angle of the (400) reflection.

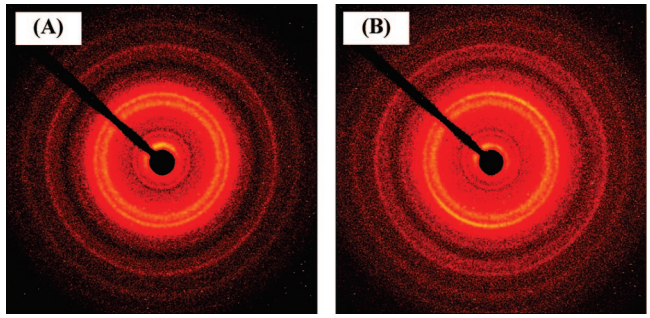

Figure 10. 2D XRD pattern of a $K_{1.8}H_{2.2}Nb_6O_{17}\cdot nH_2O$/silica gel. (A) Sample gelled in zero magnetic field and (B) in a 11.74 T field.

expressed by Hermans Orientation Parameter (f) which represents the average orientation of a pole relative to some reference orientation and can be estimated from observed diffraction intensity as a function of azimuthal angle ϕ for a selected Bragg reflection.[34] The parameter is based on the second-order Legendre function of cos ϕ and has the value 1, 0, or $-1/2$ for parallel, random, or perpendicular alignment relative to the reference orientation, respectively.

The (400) reflection for the aligned sample measured as shown in Figure 9 (same as Figure 5C) was used for calculation of the orientation parameter and the peak of the intensity distribution at $\phi = 232$ was used as the reference orientation. In this configuration, the reference orientation is parallel to the applied field. The calculated value of f is especially sensitive to the choice of baseline to the peak of the intensity vs ϕ distribution shown for (400) in Figure 9. The critical issue in baseline choice is whether or not scattering intensity at ϕ positions off-peak represents poles aligned randomly or if that

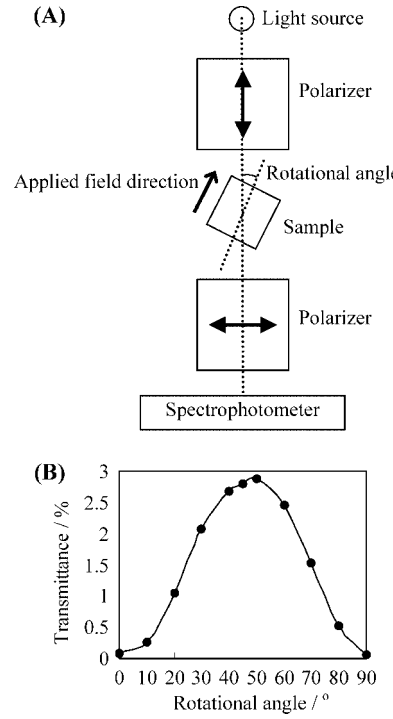

Figure 11. (A) Experimental setup for measuring sample birefringence. (B) Sample transmittance vs angle for field-aligned gels of hexaniobate nanoscrolls. Samples were positioned between crossed polarizers as shown in A.

intensity is from diffuse, amorphous, fluorescent, or other non-Bragg scattering. If baseline choice disgards random alignments, the orientation parameter is inflated and indicates more alignment than actually present. Including non-Bragg scattered intensity results in an orientation parameter that expresses less alignment than present. Examination of the 2D scan in Figure 9 indicates that there is little Bragg diffraction from (400) at ϕ positions outside of the range of the peak in the azimuthal distribution. Azimuthal integrations of intensity at background positions just to the high and low side values of the Bragg angle for (400) are shown in Figure 9 and show intensity equal to the baseline of the (400) azimuthal peak. Furthermore, intensity vs 2θ scans derived from the 2D data by azimuthal integration do not show a (400) peak when the azimuthal integration ranges include all ϕ angles not encompassed by the distribution peak shown in Figure 9. The average of intensity at high and low Bragg positions at each azimuth was subtracted from the (400) azimuthal intensity distribution for baseline correction in the calculation of the orientation parameter. The calculated value for f ranged from 0.85 to 0.92 depending on exact choice of background positions and range of azimuthal integration (90 or 180°). These values represent a high degree of alignment in the samples gelled in the applied magnetic field.

Magnetic Field Alignment of Nanoscrolls. The 2D XRD patterns of nanoscroll samples gelled with and without an applied 11.74 T field are shown in Figure 10. The sample gelled in zero field shows homogeneous diffraction rings. For the sample gelled in the field, the 002 reflection is condensed into broad arcs that are concentrated along the field direction, whereas the 220 reflection appears as a homogeneous ring.

Previous studies have shown that the sheets prefer to scroll along low Miller index directions. The 002 line, which appears as broad arcs in Figure 10B, is the strongest line in the 1D diffraction patterns of the scrolls, implying that in many of the scrolls the c-axis is the long axis. Although the degree of

orientation cannot be estimated easily from the 2D XRD data given the crystallographic heterogeneity of the nanoscrolls, the observation of arcs suggests a preference for orientation of the long axis along the field direction. This is consistent with the picture obtained for field-oriented microcrystals, illustrated in Figure 6.

Further evidence for preferred orientation of the nanoscrolls in gels prepared in the magnetic field comes from the optical birefringence measured by using a crossed polarizer and analyzer. Samples were placed in a Hewlett-Packard 8452A diode array spectrophotometer between crossed polarizers, and the sample was rotated as shown in Figure 11A. The transmittance at 600 nm is plotted vs sample angle in Figure 11B. The transmittance was near zero when the direction of applied field was 0 or 90°, and it reached a maximum near 45°. This is the behavior expected if the nanoscrolls orient preferentially parallel or perpendicular to the applied field.

Conclusions

2D and 1D XRD data show that microcrystals of the lamellar proton conductor $K_{1.8}H_{2.2}Nb_6O_{17}\cdot nH_2O$ can be aligned with a high degree of order in a strong homogeneous magnetic field and that the crystallographic *a* axis is oriented along the magnetic field direction. By gelling the aligned microcrystals using a silica sol−gel reaction, a composite material is made in which the stacking axis (the crystallographic *b* axis) is aligned perpendicular to the magnetic field. This is the desired edge-on orientation for proton-conducting membranes. In the case of nanoscrolls of the same material, there is some evidence for field-induced alignment from optical birefringence, but it could not be quantified by XRD. This is consistent with preliminary observations we have made of the magnetic alignment exfoliated layer perovskite sheets that contain paramagnetic lanthanide ions.[35]

So far, these materials have been studied as gels that contain relatively small amounts of the microcrystals or nanoscrolls in a silica matrix, which is presumably nonconducting. The volume of the silica component is approximately twice that of the microcrystals or nanoscrolls. Lower silica volume fractions gave mechanically unstable, cracked gels upon drying. An important prerequisite to testing these materials as proton-conducting membranes is to develop a gelation method that increases the volume fraction of the active component. This may be possible by using niobate rather than silica gels, followed by postprocessing to crystallize the gel fraction, or by combining magnetic alignment with gravitational, capillary, or electrophoretic forces[17–19] that could lead to more dense composites. Because a high orientation parameter is observed using a strong magnetic field, it will also be interesting to see if fields in the range of 1−2 T, which are easily generated in the laboratory, are sufficient to induce alignment of proton-conducting microcrystals. These questions will be explored in future experiments.

Acknowledgment. This work was supported by the National Science Foundation under Grant CHE-0616450 and by the Japan Society for the Promotion of Science. We thank Alan Benesi and Bernie O'Hare for their help with operation of the NMR, Henry Gong for performing the ICP-AES analysis, and Ron Heddon for providing advice and a spreadsheet to calculate *f*. The Bruker SMART APEX instrumentation was provided by NSF Chemistry Research Instrumentation and Facilities Grant CHE-0131112.

References and Notes

(1) Iwahara, H.; Uchida, H.; Ono, K.; Ogaki, K. J. *Electrochem. Soc.* **1988**, *135*, 529–533.
(2) Howe, A. T.; Shilton, M. G. *J. Solid State Chem.* **1979**, *28*, 345–61.
(3) Krogh Andersen, E.; Krogh Andersen, I. G.; Knakkergaard Moeller, C.; Simonsen, K. E.; Skou, E. *Solid State Ionics* **1982**, *7*, 301–306.
(4) Sato, M.; Jin, T.; Uematsu, K. *J. Solid State Chem.* **1993**, *102*, 557–561.
(5) Thangadurai, V.; Shukla, A. K.; Gopalakrishnan, J. *Solid State Ionics* **1994**, *73*, 9–14.
(6) Thangadurai, V.; Weppner, W. *J. Mater. Chem.* **2001**, *11*, 636–639.
(7) (a) Nowick, A.; Du, Y.; Liang, K. *Solid State Ionics* **1994**, *69*, 117–120. (b) Du, Y.; Nowick, A. S. *Solid State Ionics* **1996**, *91*, 85–91.
(8) Alberti, G.; Casciola, M.; Costantino, U.; Leonardi, M. *Solid State Ionics* **1984**, *14*, 289–295.
(9) Boysen, D. A.; Uda, T.; Chisholm, C. R. I.; Haile, S. M. *Science* **2004**, *303*, 68–70.
(10) Yamaguchi, S.; Shishido, T.; Yugami, H.; Yamamoto, S.; Hara, S. *Solid State Ionics* **2003**, *291*, 162–163.
(11) Fang, M.; Kim, C. H.; Mallouk, T. E. *Chem. Mater.* **1999**, *11*, 1519.
(12) England, W. A.; Cross, M. G.; Hamnett, A.; Wiseman, P. J.; Goodenough, J. B. *Solid State Ionics* **1980**, *1*, 231–249.
(13) Sarkar, P.; Nicholson, S. *Appl. Phys. Lett.* **1992**, *61*, 492–494.
(14) Suzuki, T. S.; Sakka, Y.; Kitazawa, K. *Adv. Eng. Mater.* **2001**, *3*, 490–492.
(15) Yamato, M.; Aoki, H.; Kimura, T.; Yamamoto, I.; Ishikawa, F.; Yamaguchi, M.; Tobita, M. *Jpn. J. Appl. Phys.* **2001**, *40*, 2237–2240.
(16) Lemaire, B. J.; Davidson, P.; Ferre, J.; Jamet, J. P.; Petermann, D.; Panine, P.; I.; Dozov, I.; Jolivet, J. P. *Eur. Phys. J. E* **2004**, *13*, 291–308.
(17) Uchikoshi, T.; Suzuki, T. S.; Okuyama, H.; Sakka, Y., J. *Mater. Res.* **2003**, *18*, 254–256.
(18) Uchikoshi, T.; Suzuki, T. S.; Okuyama, H.; Sakka, Y.; Nicholson, P. S. J. *Eur. Ceram. Soc.* **2004**, *24*, 225–229.
(19) Uchikoshi, T.; Suzuki, T. S.; Fang, F.; Okuyama, H.; Sakka, Y. *Ceram. Int.* **2004**, *30*, 1975–1978.
(20) Kimura, T.; Yoshino, M. *Langmuir* **2005**, *21*, 4805–4808.
(21) Kimura, T.; Kimura, F.; Yoshino, M. *Langmuir* **2006**, *22*, 3464–3466.
(22) Kimura, T.; Uemura, T.; Kimura, T.; Takagi, S.; Inoue, H. *Macromol. Symp.* **2006**, *242*, 120–125.
(23) Uyeda, C.; Ohtawa, K.; Okita, K.; Uyeda, N. *J. Phys. Soc. Jpn.* **2001**, *70*, 889–892.
(24) Uyeda, C.; Ohtawa, K.; Okita, K. *Jpn. J. Appl. Phys.* **2000**, *39*, L514–L517.
(25) Uyeda, C.; Tanaka, K. *J. Phys. Soc. Jpn.* **2003**, *72*, 2334–2337.
(26) Nassau, K.; Shiever, J. W.; Bernstein, J. L. J. *Electrochem. Soc.* **1969**, *116*, 348–353.
(27) Gasperin, M.; Le Bihan, M. T. J. *Solid State Chem.* **1982**, *43*, 346–353.
(28) Saupe, G. B.; Waraksa, C. C.; Kim, H.-N.; Han, Y. J.; Kaschak, D. M.; Skinner, D. M.; Mallouk, T. E. *Chem. Mater.* **2000**, *12*, 1556–1562.
(29) Du, G.; Chen, Q.; Yu, Y.; Zhang, S.; Zhou, W.; Peng, L.-M. J. *Mater. Chem.* **2004**, *14*, 1437–1442.
(30) Kobayashi, Y.; Hata, H.; Salama, M.; Mallouk, T. E. *Nano Lett.* **2007**, *7*, 2142–2145.
(31) (a) Abe, R.; Shinohara, K.; Tanaka, A.; Hara, M.; Kondo, J.; Domen, K. J. *Mater. Res.* **1998**, *13*, 861–865. (b) Abe, R.; Shinohara, K.; Tanaka, A.; Hara, M.; Kondo, J.; Domen, K. *Chem. Mater.* **1997**, *9*, 2179–2184.
(32) Kimura, T. *Polym. J.* **2003**, *35*, 823–843.
(33) Itoh, T.; Shichi, T.; Yui, T.; Takagi, K. J. *Colloid Interface Sci.* **2005**, *291*, 218–222.
(34) Hermans, P. H.; Platzek, P. *Kolloid Z.* **1939**, *87*, 246–248.
(35) Ida, S.; Ogata, C.; Eguchi, M.; Youngblood, W. J.; Mallouk, T. E.; Matsumoto, Y. *J. Am. Chem. Soc.* **2008**, *130*, 7052–7059.

JP802702M